DOI: 10.1002/cphc.201101020

On the Mechanisms of Ni-Catalysed Graphene Chemical Vapour Deposition

Robert S. Weatherup,*[a] Bernhard C. Bayer,[a] Raoul Blume,[b] Carsten Baehtz,[c] Piran R. Kidambi,[a] Martin Fouquet,[a] Christoph T. Wirth,[a] Robert Schlögl,[d] and Stephan Hofmann[a]

The development of a scalable, economical production technique for mono- and few-layer graphene (M-/FLG) is a key requirement to exploit its unique properties for applications. Catalytic chemical vapour deposition (CVD) has emerged as one of the most promising and versatile methods for M-/FLG growth. The generic principle of catalytic, rather than pyrolytic, CVD is to expose a catalyst template to a gaseous precursor at temperatures/conditions for which the precursor preferentially dissociates on the catalyst. Hence, the catalyst is key to M-/FLG formation, in particular its role in precursor dissociation, C dissolution, M-/FLG nucleation and domain growth/merging. Although the structure of as-formed graphitic layers on crystalline transition metal surfaces under ultra-high vacuum conditions has been extensively studied in surface science,[1,2] a central question remains: what M-/FLG quality can be achieved with CVD, in particular, if for cost effectiveness sacrificial polycrystalline metal films/foils and less stringent vacuum/CVD process conditions are used. There have been numerous recent reports of large area M-/FLG CVD on for instance poly-crystalline Ni[3] and Cu,[4] including integrated roll-to-roll processing.[5] However, there is currently very limited understanding of the detailed growth mechanisms,[6] and the mostly empirical process calibrations provide little fundamental insight in to how the process and M-/FLG quality/domain size can be optimised.[7]

Herein, we study M-/FLG CVD by complementary in situ probing under realistic process conditions with the aim of revealing the key growth mechanisms. We focus on poly-crystalline Ni films and simple one-step hydrocarbon exposure conditions. However, as highlighted by Figure 1, even for such seemingly simple CVD conditions, the parameter space is manifold which leads to ambiguity in the interpretation of post-growth process characterisation and motivates our in situ approach. For catalyst metals with a high C solubility, such as Ni, current literature typically assumes C precipitation upon cooling as the main growth process.[3,8] M-/FLG precipitation has been studied in detail for slow, near thermodynamic equilibrium thermal cycling of C doped crystals.[2,9] For CVD, however, the conditions are distinctly different (Figure 1): an isothermal C precursor exposure phase, which represents a variation in composition rather than temperature, is followed by a typically fast cooling or thermal quenching. Hence kinetic aspects are important. Additionally, competing processes might influence the growth outcome such as etching of M-/FLG in a reactive atmosphere, for example, hydrogen or water, during the CVD process.[10,11]

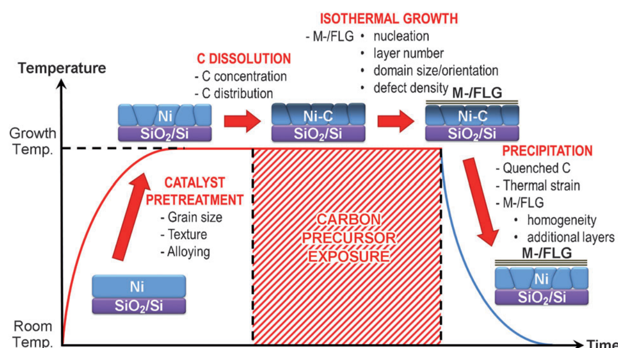

Figure 1. Illustrative processing profile for a simple one-step hydrocarbon exposure consisting of four major phases: catalyst pretreatment, C dissolution into the catalyst during initial precursor exposure, isothermal M-/FLG growth with continued precursor exposure, M-/FLG growth by precipitation upon cooling. The key catalyst and M-/FLG properties that may be defined at each phase of growth are also listed.

By combining in situ, time- and depth-resolved X-ray photoelectron spectroscopy (XPS) and in situ X-ray diffraction (XRD), we can clearly show that M-/FLG growth occurs during isothermal hydrocarbon exposure and is not limited to a precipitation process upon cooling. While the fraction of M-/FLG due to isothermal growth and precipitation upon cooling strongly depends on process conditions, we show that the former is dominant for the low-temperature CVD conditions used. We find that M-/FLG nucleation is preceded by an increase in (subsurface) dissolved C with the formation of a solid solution of C in the Ni film, which indicates that graphene CVD is not a purely surface process. We discuss our data here in the context of simple considerations of C solubility and diffusivity as well as rate equations of the basic contributing processes, in order to establish a framework to guide future improvements in graphene CVD by a more fundamental understanding.

We perform in situ XPS during low-pressure CVD of M-/FLG from hydrocarbon precursors on Ni(550 nm) films. Figure 2A

[a] R. S. Weatherup, B. C. Bayer, P. R. Kidambi, M. Fouquet, Dr. C. T. Wirth, Dr. S. Hofmann
Department of Engineering, University of Cambridge
9 JJ Thomson Avenue, Cambridge
CB3 0FA (United Kingdom)
Fax: (+44) 1223-748348
E-mail: rsw31@cam.ac.uk

[b] Dr. R. Blume
Helmholtz-Zentrum Berlin für Materialien und Energie
12489 Berlin (Germany)

[c] Dr. C. Baehtz
Institute of Ion Beam Physics and Materials Research
Helmholtz-Zentrum Dresden-Rossendorf,
01314 Dresden (Germany)

[d] Prof. R. Schlögl
Department of Inorganic Chemistry
Fritz Haber Institute of the Max Planck Society,
Faradayweg 4-6, 14195 Berlin (Germany)

 WILEY ONLINE LIBRARY © 2012 Wiley-VCH Verlag GmbH & Co. KGaA, Weinheim

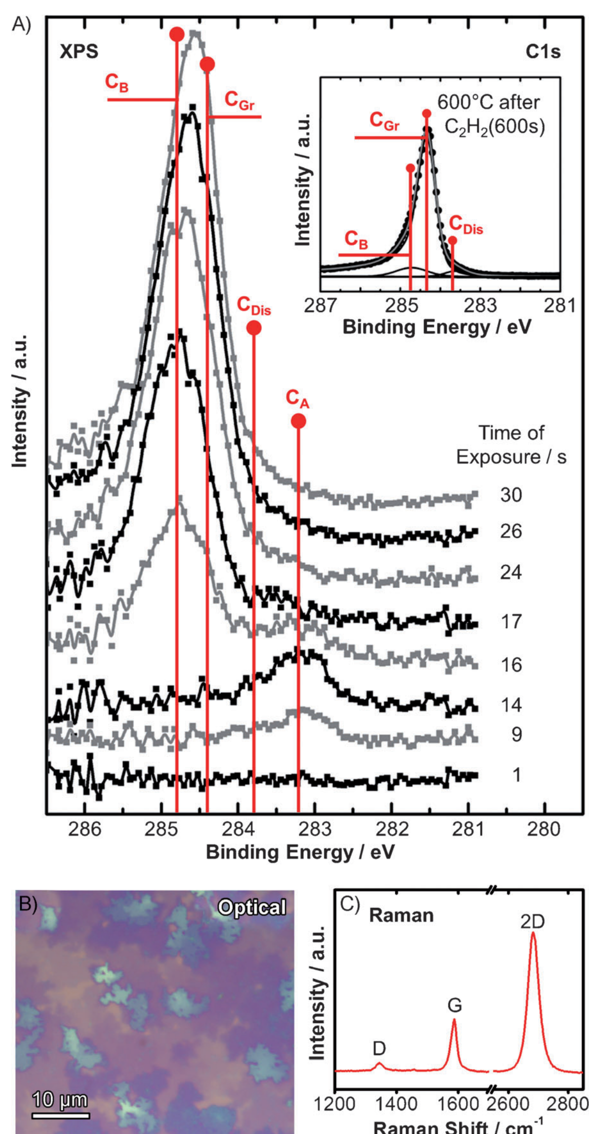

Figure 2. A) Time-resolved in situ XPS C1s core level lines for Ni(550 nm) during low-pressure CVD [base pressure 5×10^{-7} mbar, 600 °C, C_2H_2($\sim10^{-5}$ mbar), cooled at ~50 °Cmin^{-1}]. Time signatures are relative to when the C_2H_2 valve is opened and spectral acquisition begins, however exposure pressure is not instantaneously reached. Inset: A fitted C1s spectrum measured at 600 °C with C_2H_2 removed after a 600 s exposure. The spectrum is fitted using Doniach-Šùnjić functions convoluted with Gaussian profiles with an accuracy of ~0.05 eV and is background corrected (Shirley). All spectra are collected in normal emission geometry at photon energies of 435 eV (surface sensitive; $\lambda_{escape} \approx 7$ Å) with a spectral resolution of ~0.3 eV. B, C) Optical image and Raman spectra (532 nm excitation) of transferred M-/FLG film grown by low pressure CVD [base pressure 5×10^{-7} mbar, 600 °C, C_2H_2(2×10^{-6} mbar), 210 s, cooled at 25 °Cmin^{-1}]

shows the time-resolved evolution of the C1s core level spectra during C_2H_2 exposure at ~600 °C. We have previously identified four principal components in the C1s spectra at approximately 283.2 eV (C_A), 283.8 eV (C_{Dis}), 284.4 eV (C_{Gr}) and 284.8 eV (C_B), which can be consistently assigned for Figure 2A.[12,13] Shortly after the start of the C_2H_2 exposure, we observe the appearance of C bound to high reactivity Ni surface sites (C_A) which reflects the presence of C on the Ni surface originating from the decomposition of C_2H_2. This surface C diffuses into the Ni sub-surface forming an interstitial Ni-C solid solution (C_{Dis}). The C concentration increases with time until it reaches a level at which M-/FLG (C_{Gr}) nucleates isothermally at the Ni surface. XPS measurements of initially pristine HOPG following a variety of Ar^+ plasma treatments show that a C_B peak can be induced (alongside the existing C_{Gr} peak) that is attributed to the formation of sp^3 and dangling bonds. C_B can thereby be assigned to deleterious sp^3-bonded C or C at the periphery of graphene/FLG domains. Hence C_B initially dominates, while C_{Gr} becomes increasingly prominent as growth proceeds.

We observe the same C1s evolution during ethylene exposures [base pressure 5×10^{-7} mbar, 600 °C, C_2H_4($\sim10^{-5}$ mbar)], indicative of the same growth mechanisms with the major difference being a much longer incubation time (~300 s) before the appearance of the characteristic C1s signature, which will be discussed later. Figure 2B,C show an optical image and corresponding Raman spectra of a representative as-grown M-/FLG film transferred to a SiO_2(300 nm)/Si substrate, highlighting the graphitic quality and the variation in the number of graphene layers.

During our in situ XPS measurements of Ni films, we found that exposing already grown M-/FLG to H_2(~1 mbar) whilst still at the growth temperature resulted in the gradual removal of the species observed in the C1s XP spectra. The M-/FLG did not return on removal of the H_2 gas feed indicating that etching of the M-/FLG had occurred, and suggesting a competing etching process for CVD conditions where hydrogen is also present during precursor exposure or cooling, which has previously been suggested for Ni catalysts.[10] We note that this etching could also arise from residual water or oxygen contamination.[14]

Figures 3A,B show depth-resolved $Ni2p_{3/2}$ XP spectra measured at salient points of the growth process. Two main components can be identified at ~852.6 and 853.0 eV, which correspond to metallic Ni (Ni_M) and the Ni–C solid solution (Ni_{Dis}), with the latter directly related to the C_{Dis} peak seen in the C1s spectra.[12] Prior to C_2H_2 exposure, predominantly metallic Ni is present at the catalyst surface with only a small Ni_{Dis} component associated with residual C contamination (Figure 3A). Immediately following the exposure, Ni_{Dis} is stronger in intensity for the surface sensitive scans, reflecting an increase in dissolved C due to the growth process. The corresponding "bulk" sensitive spectrum (Figure 3B) shows a much stronger Ni_{Dis} component for the catalyst subsurface and thus indicates that the dissolved C is not solely a surface species and that a growth mechanism based on the in-plane transformation of a monolayer of surface-carbide, as seen at lower growth temperatures (<460°C)[15] is not readily apparent. On cooling of the sample to 200 °C, Ni_{Dis} is seen to further increase near the catalyst surface (Figure 3A) which we attribute to C diffusing from the Ni bulk towards the catalyst surface at the chosen cooling rate (~50 °Cmin^{-1}). Figure 3C shows the C1s spectra measured just after C_2H_2 exposure at the growth temperature, and following cooling to room temperature. A modest increase in the C1s intensity, compared to that at the end of isothermal C_2H_2 exposure, is observed which is attributed to the expected C precipitation from the Ni-C solid solution.

 © 2012 Wiley-VCH Verlag GmbH & Co. KGaA, Weinheim

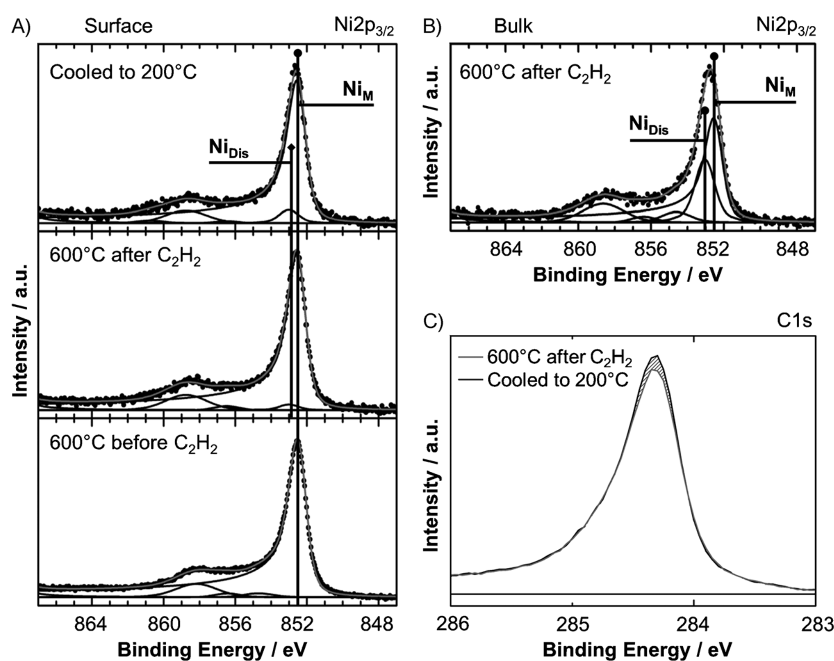

Figure 3. Depth-resolved in situ XPS $Ni2p_{3/2}$ core level lines for Ni(550 nm) film during low pressure CVD (conditions as in Figure 2A with a spectral resolution of ~0.3–0.4 eV). A) Surface-sensitive spectra acquired at 600 °C before and after precursor exposure, and on cooling to 200 °C, collected at photon energies of 1010 eV ($\lambda_{escape} \approx 7$ Å). B) Bulk-sensitive spectrum acquired at 600 °C after precursor exposure at photon energies of 1300 eV ($\lambda_{escape} \approx 10$ Å). Increased information depth is achieved using higher incident X-ray energies and hence increased electron mean free path lengths. C) XPS C1s core level lines for Ni (550 nm) following precursor exposure (conditions as in Figure 2A) acquired at 600 °C and after cooling to 200 °C, at photon energies of 435 eV. The spectra are fitted using Doniach–Šùnjić functions convoluted with Gaussian profiles with an accuracy of ~0.05 eV. All spectra are background-corrected (Shirley) and collected in normal emission geometry.

Complementary to the surface-sensitive XPS, we use in situ grazing-incidence XRD with an estimated information depth of ~50 nm to study the growth process. Figure 4A shows diffractograms acquired at the important stages of the Ni catalysed M-/FLG CVD. Heating of the catalyst films in vacuum, leads to sharpening of the Ni reflections, indicating significant grain growth and that prior to C precursor exposure the catalyst is metallic and of face-centred-cubic (fcc) structure. On C_2H_2 exposure at constant temperature, a graphite (0 0 2) reflection emerges confirming the isothermal growth of M-/FLG seen in the in situ XPS measurements. The graphite (0 0 2) reflection increases in intensity with continuing exposure, but as soon as the C_2H_2 precursor is removed no further increase is observed for isothermal conditions.[12] Figure 4B shows time-resolved reflection intensity measurements of the graphite (0 0 2) and Ni_3C(1 1 3) reflections for an extended 1200 s exposure. No (even transient) reflection associated with Ni_3C emerges,[16] and we note that no other reflections related to Ni-carbide are observed throughout our experiments precluding the presence of a bulk, crystalline Ni-carbide during the M-/FLG growth. Figure 4B further shows that graphitic growth proceeds with continuing exposure, whereby the curve for the graphite intensity can be fitted by two exponential functions. The graphite growth will eventually terminate and we expect this to be related to the increasing graphite layer thickness blocking the precursor supply to the Ni catalyst.

XRD also allows us to monitor the variation of the Ni lattice parameter throughout the CVD process. We extract lattice parameters using full pattern LeBail fitting and correct for thermal expansion by extracting the thermal expansion coefficient for a temperature range of 500–600 °C under vacuum. Upon isothermal C_2H_2 exposure at ~550 °C we observe an irreversible shift in the Ni peak positions associated with an increase of lattice parameter. To confirm this lattice expansion is caused by C dissolution, experiments were performed for H_2 exposures using Ni films in the range 450–750 °C. It was found that exposure to H_2 (~1 mbar) leads to a lattice expansion that is reversed on isothermally returning to vacuum (~10^{-5} mbar), and at H_2 pressures similar to the C_2H_2 exposure no noticeable expansion due to H_2 alone could be observed. Therefore, the increase of 0.0010 ± 0.00016 Å is attributed to the formation of an interstitial Ni–C solid solution, which directly relates to the C_{Dis}/Ni_{Dis} components observed in the XPS measurements. Zwell et al. obtained an expression for the variation in Ni lattice parameter (a_0) with C concentration (x) of a_0 (Å) $= 3.5238 + 0.0074x$ (atom %) for samples quenched to room temperature.[17] Assuming the same change in lattice parameter with C concentration for our growth conditions, we calculate that the expansion we observe corresponds to 0.14 ± 0.02 atom % C.

Our in situ measurements indicate that under the chosen conditions, M-/FLG CVD occurs predominantly via isothermal growth rather than precipitation upon cooling. This can be put into context via some very simplistic considerations of bulk, equilibrium carbon solubility (*S*), and carbon diffusivity (*D*) in fcc Ni, which can be parameterised as $S = 5.33 \times 10^{28} \exp(-4885/T)$ atoms m^{-3} (converting from the wt % measurements of Lander et al.[18]) and $D = 2.48 \times 10^{-4} \exp(-20200/T)$ $m^2 s^{-1}$.[18] The former estimates the saturated C content as 0.16 atom % at 550 °C, which correlates well with our extrapolated value for the in situ XRD measurements. Table 1 summarises estimates of saturated C content and of total amount of C able to diffuse to the Ni surface for a range of temperatures and cooling rates. The quantities of C are given in monolayer graphene units (ML), whereby S is multiplied by a fixed catalyst thickness of 550 nm. It is evident that for low temperatures and typical cooling rates used here, no significant M-/FLG growth can be expected based on a precipitation upon cooling mechanism. Our experiments show the growth of five gra-

 © 2012 Wiley-VCH Verlag GmbH & Co. KGaA, Weinheim

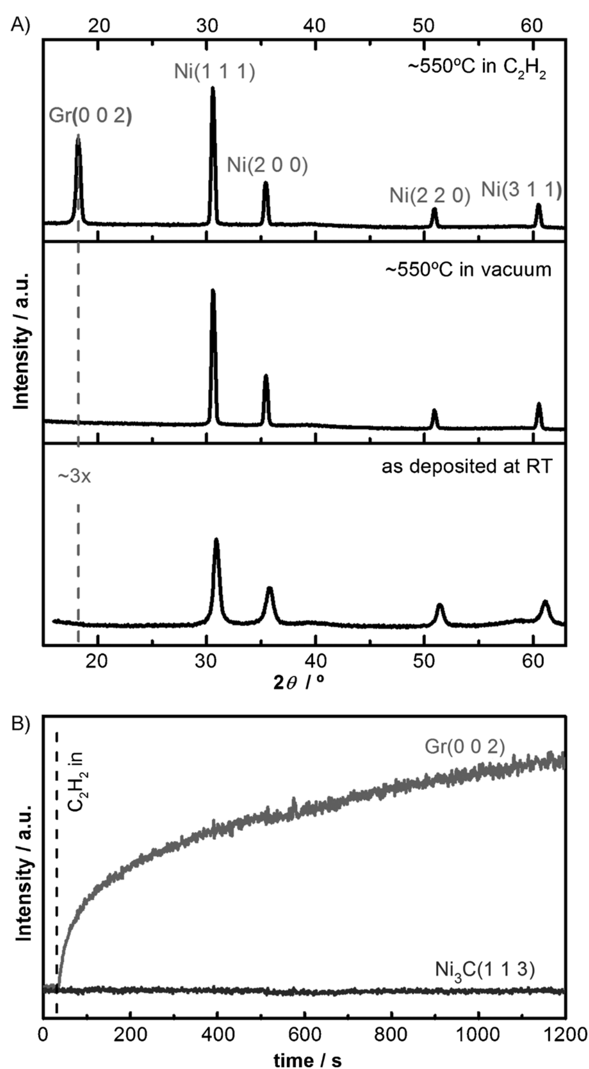

Figure 4. A) In situ XRD diffractograms of Ni(170 nm)/SiO_2(200 nm)/Si as deposited, at a growth temperature of 550 °C before C precursor exposure in vacuum(10^{-5} mbar) and during C_2H_2(10^{-3} mbar) exposure after 1200 s. Acquisition time per scan ~25 min. B) Time-resolved plot of graphite(0 0 2) and Ni_3C(1 1 3) peak intensities for Ni(~170 nm)/SiO_2(200 nm)/Si for C_2H_2 (10^{-3} mbar) exposure at 550 °C for 1200 s. A monochromatic X-ray beam of 11.5 keV, and a wavelength of 1.07812 Å [selected by a Si(1 1 1) double crystal monochromator] with an incident angle of $\alpha_i = 0.5°$ was used.

phene layers or more for one-step hydrocarbon exposure conditions at for instance 450 °C, whereas Table 1 estimates an arrival of only a fraction of a monolayer upon cooling to room temperature. This is consistent with the small increase in C1s intensity after cooling in Figure 3 B and clearly supports our conclusion that isothermal growth is dominant here. Table 1 also suggests that the contribution of precipitation upon cooling becomes greater for higher growth temperatures and that it becomes challenging to avoid the precipitation of multiple graphene layers for 1000 °C at realistic cooling rates. It should be noted that growth by precipitation inherently involves M-/FLG formation at lower temperatures than the dosing temperature, whereas for isothermal growth the M-/FLG is formed at the dosing temperature. Furthermore, accelerated diffusion

Table 1. Saturation C content for a Ni(550 nm) film and estimates of the total quantity of C that diffuses to the film's surface on cooling for some typical constant cooling rates and growth temperatures.[8,9,12,20]

Growth Temperature [°C]	Saturation C content [ML][a]	Estimate of total C that diffuses to the Ni surface on cooling to 20 °C [MLs][a,b]		
		0.01 °C min^{-1}	50 °C min^{-1}	1800 °C min^{-1}
450	0.89	0.73	0.07	0.01
600	2.85	2.69	1.73	0.52
1000	16.54	16.38	15.42	14.04

[a] Number of monolayers of graphene assuming an atomic layer density of 3.8×10^{19} C atoms m^{-2}. [b] Quantity of C diffused at a given cooling rate was calculated by numerical integration assuming instantaneous cooling steps every 1 °C between the growth temperature and 20 °C with an appropriate dwell time at each step to give the required cooling rate. For each step the change in S and the effective diffusion length $2\sqrt{\sum D_i t}$ based on the remaining cooling ramp was calculated. *S* and *D* as functions of temperature were based on ref. [18]. It was assumed that only C from a depth equal to the L_e diffuses to the exposed Ni surface, and that all C above the solubility limit diffuses to the exposed Ni surface when L_e exceeds the Ni film thickness (550 nm).

through grain boundaries might play a more dominant role for C precipitation upon cooling[19] compared to the constant hydrocarbon exposure conditions during isothermal growth. Hence more uniform and higher quality graphitic films may be expected from isothermal growth.

For the CVD conditions highlighted in Figure 1, the presented in situ XPS and XRD results reveal the following coherent growth model: Upon heating to the growth temperature and subsequent annealing, grain growth in the Ni catalyst film occurs combined with a significant evolution in microstructure and texture. The Ni surface mobility can thereby for instance be increased by a H_2 atmosphere, which we found to greatly reduce roughening of the catalyst films compared to annealing in vacuum. On introduction of the gaseous carbon precursor, the precursor dissociates at the catalyst surface and C begins to diffuse into the catalyst film. XRD shows that no, even transient, bulk carbide is formed. XPS shows that the amount of C dissolved in the subsurface rises with continuing exposure, until it reaches a level at which M-/FLG nucleates isothermally on the exposed catalyst surface. The nucleation density, and related domain size of the graphene films produced can thus be influenced, by for example the C precursor pressure as well as various pre-treatments of the catalyst film such as alloying or annealing.[12] XRD indicates that at a later stage of growth the C content in the bulk Ni closely matches the bulk solubility limit. We emphasise, however, that we have no direct measurement of the C bulk content at the point of M-/FLG nucleation. A consideration of local (sub)surface C super-saturations would have to include rate equations for: 1) the impingement precursor flux and rate of catalytic dissociation; 2) M-/FLG nucleation barriers and C incorporation rates; and 3) C diffusion rates into the catalyst bulk. Taking simple assumptions for (1), that is, kinetic gas model and sticking coefficient of one for C_2H_2, and the values of saturation C content given in Table 1, one can estimate that it would take about 3 s to fill the Ni(~550 nm) film at 600 °C and a 10^{-5} mbar C_2H_2 exposure to its C solubility

 © 2012 Wiley-VCH Verlag GmbH & Co. KGaA, Weinheim

limit. A significantly lower sticking coefficient for C_2H_4 could explain the observed longer incubation times. The aforementioned kinetic aspects combined with the C reservoir size can result in a significant dependence of graphene CVD on catalyst film thickness. Assuming, for instance, that all catalytically dissociated C [process (1)] can initially diffuse into the catalyst bulk [process (3)], a significant increase in incubation time with increasing catalyst film thickness is expected, which we indeed observe when comparing Ni(550nm) thin films with 25 µm thick Ni foils for low-exposure conditions. We note, however, that C saturation of the catalyst bulk is not a necessity for M-/FLG nucleation and that a rate inequality between processes (1) and (3) can also result in the required C supersaturation at the catalyst surface.

As shown in Figure 4, the rate of isothermal graphite growth slows down with increasing exposure time, which is likely to be due to the increasing graphite coverage blocking the precursor supply to the Ni catalyst. After the precursor exposure, further M-/FLG growth may occur from C precipitating on cooling (Figure 1) due to the reduction of C solubility in the catalyst, but as shown the extent of this contribution is dependent on the cooling rate and is found to decrease substantially with the lowering of the growth temperature.

Our complementary in situ methodology has enabled a coherent growth model for catalytic graphene formation on Ni films to be developed, which we anticipate will be of use in the rational optimisation of graphene CVD. We note that the growth model presented here may be generally applicable to carbon nanostructures, and that our in situ approach may be valuable for other catalyst/nanomaterial systems.

Experimental Section

Ni films (550 nm or 170 nm) were sputter-deposited on to SiO_2(300 nm)/Si substrates using a custom-built RF magnetron sputter deposition system. Ni thickness was measured using mechanical profilometry. The samples were annealed and exposed to hydrocarbons in custom-built cold-wall reactors at low pressures [base pressures 5×10^{-7} mbar, ~600 °C, C_2H_2(2×10^{-6} mbar), cooled at ~25–100 °C min^{-1}].

In situ XPS measurements during low-pressure CVD were performed at the BESSY II synchrotron at the ISISS end station of the FHI-MPG. An IR laser focused onto an SiC backplate was used for sample heating. Temperature readings were taken from a thermocouple spot-welded in the vicinity of the sample and, as such, this may lead to an uncertainty in the actual sample temperature of ~50 °C. In situ (grazing-incidence) XRD during low-pressure CVD was performed at the European Synchrotron Radiation Facility (beamline BM20/ROBL, operated by the Helmholtz-Zentrum Dresden–Rossendorf). Diffracted X-rays were measured using a horizontally aligned Soller slit system and a scintillation detector. A boron nitride coated graphite resistive heating element was used for sample heating, and temperature was measured with a thermocouple in direct contact with part of the sample surface.

The presence of M-/FLG following growth was confirmed using scanning electron microscopy (SEM, FEI Philips XL30 s, 1 kV) on the as-grown films and optical microscopy and Raman spectroscopy (Renishaw Raman InVia Microscope, 532 nm excitation) on M-/FLG transferred to SiO_2(300 nm)/Si substrates. Transfer was carried out using a polymethylmethacrylate (PMMA) support layer and a 0.5 M aqueous solution of $FeCl_3$ to remove the Ni catalyst layer. Acetone was then used to dissolve the PMMA support.

Acknowledgements

We acknowledge the Helmholtz-Zentrum-Berlin Electron storage ring BESSY II for provision of synchrotron radiation at the ISISS beamline and we thank the BESSY staff for continuous support of our experiments. We acknowledge the European Synchrotron Radiation Facility (ESRF) for provision of synchrotron radiation facilities and we thank the staff for assistance in using beamline BM20/ROBL. The research leading to these results has received funding from the European Community's Seventh Framework Programme (FP7/2007–2013) under Grant Agreement 226716. S.H. acknowledges funding from ERC grant InsituNANO (n°279342) and from EPSRC (Grant Nr. EP/H047565/1). PRK acknowledges funding the Cambridge Commonwealth Trust. R.S.W. acknowledges funding from EPSRC (Doctoral training award) and Sidney Sussex College.

Keywords: chemical vapor deposition · graphene · nickel · photoelectron spectroscopy · X-ray diffraction

[1] a) A. Morgan, G. Somorjai, *Surf. Sci.* **1968**, *12*, 405–425; b) J. May, *Surf. Sci.* **1969**, *17*, 267–270; c) J. Wintterlin, M. L. Bocquet, *Surf. Sci.* **2009**, *603*, 1841–1852; d) C. Oshima, A. Nagashima, *J. Phys. Condens. Matter* **1997**, *9*, 1–20.
[2] J. Shelton, H. Patil, J. Blakely, *Surf. Sci.* **1974**, *43*, 493–520.
[3] Q. Yu, J. Lian, S. Siriponglert, H. Li, Y. P. Chen, S. S. Pei, *Appl. Phys. Lett.* **2008**, *93*, 113103.
[4] X. Li, W. Cai, J. An, S. Kim, J. Nah, D. Yang, R. Piner, A. Velamakanni, I. Jung, E. Tutuc, S. K. Banerjee, L. Colombo, R. S. Ruoff, *Science* **2009**, *324*, 1312–1314.
[5] S. Bae, H. Kim, Y. Lee, X. Xu, J.-S. Park, Y. Zheng, J. Balakrishnan, T. Lei, H. Ri Kim, Y. I. Song, Y.-J. Kim, K. S. Kim, B. Özyilmaz, J.-H. Ahn, B. H. Hong, S. Iijima, *Nat. Nanotechnol.* **2010**, *5*, 574–578.
[6] X. Li, W. Cai, L. Colombo, R. S. Ruoff, *Nano Lett.* **2009**, *9*, 4268–4272.
[7] a) X. Li, C. W. Magnuson, A. Venugopal, J. An, J. W. Suk, B. Han, M. Borysiak, W. Cai, A. Velamakanni, Y. Zhu, L. Fu, E. M. Vogel, E. Voelkl, L. Colombo, R. S. Ruoff, *Nano Lett.* **2010**, *10*, 4328–4334; b) S. Lee, K. Lee, Z. Zhong, *Nano Lett.* **2010**, *10*, 4702–4707.
[8] A. Reina, X. Jia, J. Ho, D. Nezich, H. Son, V. Bulovic, M. S. Dresselhaus, J. Kong, *Nano Lett.* **2009**, *9*, 30–35.
[9] M. Eizenberg, J. Blakely, *Surf. Sci.* **1979**, *82*, 228–236.
[10] a) J. Figueiredo, *J. Catal.* **1975**, *40*, 154–159; b) J. Rostrup-Nielsen, D. L. Trimm, *J. Catal.* **1977**, *48*, 155–165.
[11] I. Vlassiouk, M. Regmi, P. Fulvio, S. Dai, P. Datskos, G. Eres, S. Smirnov, *ACS Nano* **2011**, *5*, 6069–6076.
[12] R. S. Weatherup, B. C. Bayer, R. Blume, C. Ducati, C. Baehtz, R. Schlögl, S. Hofmann, *Nano Lett.* **2011**, *11*, 4154–4160.
[13] a) S. Hofmann, R. Sharma, C. Ducati, G. Du, C. Mattevi, C. Cepek, M. Cantoro, S. Pisana, A. Parvez, F. Cervantes-Sodi, A. C. Ferrari, R. Dunin-Borkowski, S. Lizzit, L. Petaccia, A. Goldoni, J. Robertson, *Nano Lett.* **2007**, *7*, 602–608; b) S. Hofmann, R. Blume, C. T. Wirth, M. Cantoro, R. Sharma, C. Ducati, M. Hävecker, S. Zafeiratos, P. Schnoerch, A. Oestereich, D. Teschner, M. Albrecht, A. Knop-Gericke, R. Schlögl, J. Robertson, *J. Phys. Chem. C* **2009**, *113*, 1648–1656.
[14] B. C. Bayer, S. Hofmann, C. Castellarin-Cudia, R. Blume, C. Baehtz, S. Esconjauregui, C. T. Wirth, R. A. Oliver, C. Ducati, A. Knop-Gericke, A. Goldoni, C. Cepek, J. Robertson, *J. Phys. Chem. C* **2011**, *115*, 4359–4369.
[15] J. Lahiri, T. Miller, L. Adamska, I. I. Oleynik, M. Batzill, *Nano Lett.* **2011**, *11*, 518–522.

 © 2012 Wiley-VCH Verlag GmbH & Co. KGaA, Weinheim

[16] a) V. K. Portnoi, A. V. Leonov, S. N. Mudretsova, S. A. Fedotov, *Phys. Met. Metallogr.* **2010**, *109*, 153 – 161; b) Powder Diffraction File 72 – 1467. JCPDS-International Centre for Diffraction Data; Newtown Square: PA.
[17] a) L. Zwell, E. J. Fasiska, Y. Nakada, A. S. Keh, *Trans. Met. Soc. AIME* **1968**, *242*, 765 – 766; b) B. M. Singleton, P. Nash, *Bull. Alloy Phase Diagrams* **1989**, *10*, 121 – 126.
[18] J. J. Lander, H. E. Kern, A. L. Beach, *J. Appl. Phys.* **1952**, *23*, 1305 – 1309.
[19] L. Baraton, Z. B. He, C. S. Lee, C. S. Cojocaru, M. Châtelet, J.-L. Maurice, Y. H. Lee, D. Pribat, *EPL* **2011**, *96*, 46003.
[20] Y. Miyata, K. Kamon, K. Ohashi, R. Kitaura, M. Yoshimura, H. Shinohara, *Appl. Phys. Lett.* **2010**, *96*, 263105.

Received: December 18, 2012
Published online on February 29, 2012

© 2012 Wiley-VCH Verlag GmbH & Co. KGaA, Weinheim